Taylor & Francis
Taylor & Francis Group

Science and Technology of Advanced Materials: Methods

ISSN: (Print) (Online) Journal homepage: www.tandfonline.com/journals/tstm20

Dielectric tensor of perovskite oxides at finite temperature using equivariant graph neural network potentials

Alex Kutana, Koki Yoshimochi & Ryoji Asahi

To cite this article: Alex Kutana, Koki Yoshimochi & Ryoji Asahi (23 Apr 2025): Dielectric tensor of perovskite oxides at finite temperature using equivariant graph neural network potentials, Science and Technology of Advanced Materials: Methods, DOI: 10.1080/27660400.2025.2497254

To link to this article: https://doi.org/10.1080/27660400.2025.2497254

Publisher: Taylor & Francis & The Author(s). Published by National Institute for Materials Science in partnership with Taylor & Francis Group
Journal: *Science and Technology of Advanced Materials: Methods*
DOI: 10.1080/27660400.2025.2497254

Dielectric tensor of perovskite oxides at finite temperature using equivariant graph neural network potentials

Alex Kutana, Koki Yoshimochi and Ryoji Asahi✉

Nagoya University, Furo-cho, Chikusa-ku, Nagoya, Japan
✉E-mail: asahi.ryoji.d9@f.mail.nagoya-u.ac.jp

Abstract
Atomistic simulations of properties of materials at finite temperatures are computationally demanding and require models that are more efficient than the ab initio approaches. Machine learning (ML) and artificial intelligence (AI) address this issue by enabling accurate models with close to ab initio accuracy. Here, we demonstrate the utility of ML models in capturing properties of realistic materials by performing finite temperature molecular dynamics simulations of perovskite oxides using a force field based on equivariant graph neural networks. The models demonstrate efficient learning from a small training dataset of energies, forces, stresses, and tensors of Born effective charges. We qualitatively capture the temperature dependence of the dielectric tensor and structural phase transitions in calcium titanate.

Keywords
graph neural network; machine learning; dielectrics; perovskite oxides; phase transitions

1. Introduction
In atomistic simulations of realistic materials, one requires efficient models that can yield accurate properties, and at the same time are sufficiently fast to permit multiple sampling in order to acquire good statistics. At present, models based on graph convolutional neural networks (GCNNs) are some of the most promising choices to satisfy these requirements. These models have now been widely adopted for efficient modeling of properties of molecules and materials [1]. The accuracy of GCNNs can be further increased by replacing the convolution with a more general “message passing” [2], and imposing physics-informed equivariance constraints [3,4]. Equivariant message passing GNNs have been employed to implement interatomic potentials [5,6], predict spectra [7–9], reaction barriers [10], and atomic tensorial

properties [11]. Their accuracy approaches that of ab initio methods, while locality ensures linear scaling with system size, making these methods ideal for large scale atomistic simulations. In addition to improving model accuracy, geometric equivariant features naturally support tensorial output values that represent various anisotropic properties. This makes equivariant GNNs well-suited for studying materials where directional dependencies and anisotropy play an important role.

Recently, a number of ML approaches have been proposed to represent tensors of Born effective charges. Differentiable models predict Born charges as the derivatives of polarization with respect to atomic displacements. A neural network (NN) model predicting the Cartesian components of polarization and Born charge tensors from vector atomic fingerprints has been successfully utilized to study ion migration in external electric fields [12]. A deep NN utilizing sums of atomic neighborhood density functions was used to predict polarization, Born charges, and other related properties of dielectrics [13]. Kernel ridge regression has been applied to describe polarization and Born charge tensors [14] utilizing a kernel based on the covariance of a 3-dimensional atomic descriptor. A NN model representing Born charge tensors as second derivatives of the electric enthalpy has been used to study temperature-dependent response of ferroelectrics [15]. Born charge tensors have been learned directly with equivariant GNNs [11]. The dielectric response has been also modeled with random forest [16–18], gradient boosting [19], support vector regression and NNs [20], and Gaussian process regression [21].

In this work, message-passing equivariant GNNs are employed as a force field, as well as for predicting polarization from the tensors of Born effective charges, enabling the calculation of temperature-dependent anisotropic dielectric tensor from finite temperature molecular dynamics (MD) simulations. The models are also accurate enough to be able to reproduce structural phase transitions with temperature, proving to be a powerful tool for probing thermodynamic properties and phase behavior of materials under realistic conditions. Here, the main focus is on the structure and properties of the mineral perovskite, $CaTiO_3$, but the approach used should be equally applicable to other systems. Equivariant GNNs exhibit fast training from small datasets, and facile preparation of accurate specialized models fitted to any target system of interest is possible. The models can then be used for long stable molecular dynamics runs in large cells, allowing calculations that would be unfeasible with cubically scaling density functional theory (DFT) approaches.

2. Methods

MACE [6] and Equivar [11] GCNNs are used for total energy, force, and Born effective charge tensor predictions. The models utilize graph convolutional neural network [22] architectures [23], where atoms are mapped to vertices/nodes, and bonds to edges of a graph. Each node is assigned a descriptor, and each edge an attribute, represented by arrays of real numbers. The inputs (atomic identities and positions) are converted to node descriptors and edge attributes. These hidden representations are transformed during the message passing/interaction stage [2], with the number of interactions determining the depth of the GCNN. Messages can propagate beyond nearest neighbors over multiple interactions, resulting in the total receptive field of a node being larger than the nominal cutoff distance. Target values are output at the model's readout stage. In the `e3nn` implementation of E(3)-equivariant GCNNs [24], hidden representations have an additional structure, and are partitioned into the irreducible

representations of the E(3) group, while convolutions are superseded by the equivariance-preserving Clebsch-Gordan transforms [25]. Higher order convolutions have been implemented in MACE utilizing nested Clebsch-Gordan transforms [6]. MACE outputs are scalars representing the total energy, and forces on atoms are obtained via automatic differentiation of the total energy with respect to the input atomic positions. In Equivar, tensors of Born effective charges are learned directly as general rank 2 tensors, decomposed into the direct sum of representations 0e+2e+1e [11]. A cutoff radius of 6 Å with 2 interactions was used in MACE, and a cutoff of 3 Å with 6 interactions in Equivar.

Four datasets were employed for model training, labeled A, B, C, and D here. The letter suffix is also used for naming the model trained with the respective dataset. Dataset A contains energies, forces, stresses, and Born effective charges of 178 sparsified snapshot from ab initio MD simulations of Pnma $CaTiO_3$ (CTO) between 300 K and 500 K. Dataset B contains 502 snapshots of $BaTiO_3$ (BTO) at similar conditions, and dataset C 191 snapshots of $CaZrO_3$ (CZO). Dataset D is a combination of datasets A-C. Density functional perturbation theory (DFPT) calculations were performed using the VASP code [26]. The settings were similar to those used in previous works [27,18,11]. Core electrons were treated with the projector-augmented wave (PAW) method, and a plane wave basis with a cutoff of 520 eV was used for expanding valence pseudo wavefunctions. The *k* point grid density of 3000 *k* points·atom (approximately corresponding to a distance of 0.2 $Å^{-1}$ between the *k* points) was used for integrating over the Brillouin zone. Self-consistent field calculations were considered converged after satisfying the convergence threshold of 10^{-7} eV for the total energy and electronic eigenvalues. In the DFPT calculations of Born effective charge tensors, perturbation expansion after discretization (PEAD) approach [28] with finite difference stencil of order 4 was employed. PBEsol functional was used throughout, and Hubbard *U* correction of 3 eV was applied to *d* electrons in transition metals, except for Ti, where *U* = 0 was used. Message-passing atomic cluster expansion (MACE) [6] and Equivar [11] models were trained from scratch using datasets A-D for 1000 epochs. An example of a learning curve of Equivar for Born effective charges is shown in Fig. S1, demonstrating fast learning, with a dataset of size ~100 being sufficient to have a mean absolute error (MAE) of $2x10^{-2}$. For MACE, it is also found that a dataset of size ~100 is sufficient to exceed the accuracy of the foundation MACE-MP-0 model [29], underscoring the importance of the training set being close enough to the target system of interest.

Energies, forces, stress tensors, and tensors of atomic Born effective charges are obtained from MACE and Equivar models. In the linear regime with a small external electric field, the force can be calculated from the Born charge. The Born charge tensors are the derivatives of the forces on ions with respect to the external electric field: $Z^*_{\kappa,\alpha\beta} = 1/|e|\partial F_{\kappa,\beta}/\partial \mathcal{E}_\alpha$. The force $F_{\kappa,\alpha}$ acting on ion κ along the direction α is then given by:

$$F_{\kappa,\alpha}=F_{\kappa,\alpha}(\mathcal{E}=0) + |e|\Sigma_\beta \mathcal{E}_\beta Z^*_{\kappa,\beta\alpha} \quad (1)$$

Here, $\mathcal{E}_\beta$ is the applied external electric field, $|e|$ is the elementary charge, and $Z^*_{\kappa,\alpha\beta}$ is the tensor of Born effective charges. The forces at zero electric field $F_{\kappa,\alpha}(\mathcal{E}=0)$ are obtained from the MACE model, and Born effective charges from Equivar. The total energy is then given by:

$$E=E(\mathcal{E}=0) - |e|\Sigma_{\kappa,\alpha\beta} \mathcal{E}_\beta Z^*_{\kappa,\beta\alpha}\, u_{\kappa,\alpha} \quad (2)$$

with $u_{\kappa,\alpha}$ being the displacement of ion κ along direction α. The polarization is calculated from the finite field method, with change in polarization due to the displacement of ions being

$P_\alpha=(e/\Omega)\Sigma_{\kappa,\beta}Z^*_{\kappa,\alpha\beta}u_{\kappa,\beta}$. Finite temperature *NVT* MD simulations are performed with the external electric field □ =5×10^7 V/m, using a time step of 1 fs and Berendsen thermostat with a coupling time constant of 10 fs.

3. Results

Predictions of our MACE models are compared with those of the "foundation models" [29] trained on the Materials Project Trajectory (MPtrj) dataset [30]. We also compare the performance of the newly trained Equivar with the earlier BM1 model [11]. Of importance is the model's ability to capture the relevant physics of the system, in particular, to accurately reproduce the "anomalous" effective charges, which appear prominently in systems with mixed ionic-covalent bonding, such as perovskite oxides [31–33]. In perovskite titanates, the modulation of Ti 3*d* - O 2*p* orbital hybridization with interatomic distance [34,35] induces the flow of the electronic current along the Ti-O bonds, giving rise to anomalous charges [32,33]. Anomalous Born charges are a prerequisite for a large static dielectric constant [18,27], and are crucial for ferroelectricity [31,36]. The values for the anomalous charges in ABO_3 perovskites are ~7.1 for Ti, and ~-5.7 for O, whereas the "normal" charges are ~-2 for O and ~2.6 for Ca [37]. A satisfactory model must be able to predict the large anomalies in charges of Ti, vastly different charges for the two inequivalent O displacements, a mostly static charge of Ca, as well as capture the variations with atomic displacements.

Figure 1 compares model predictions with DFPT values for the evolution of the Born charges with atomic displacements in Pnma $CaTiO_3$ (CTO). The DFPT values that were used to train the models are in a good agreement with the earlier literature reports [37,38]. Note that the BM1 model [11], trained on a dataset of 1,224 perovskite, 17,991 Li_3PO_4, and 10,103 ZrO_2 structures, makes worse predictions than a specialized model with the same architecture (EquivarA) trained with only 178 $CaTiO_3$ structures. This is possibly due to the fact that no information on the Z^* variation in CTO was available in the BM1 training set, whereas the dataset used for training EquivarA consisted of MD snapshots with perturbed geometries. Both anomalous and normal charges are well captured by EquivarA and EquivarD, whereas BM1 predictions sometimes deviate, e.g., by overestimating the decrease of the O charge with displacement. EquivarD, trained on a slightly more diverse chemistry, exhibits larger error than EquivarA, possibly due to regularization. The anomalous charges in CTO are seen to attain maximum values near the equilibrium positions.

A range of custom MACE [6] force field models has been trained to perform MD simulations, and their performance compared with that of MACE-MP-0 [29]. Figure 2a benchmarks force predictions of MACE-MP-0, as well as MACE models trained from scratch using the CTO dataset. In the latter case, a 5-fold cross-validation was carried out using the CTO dataset with 178 geometries. Despite the small dataset size, a specialized model significantly outperforms the generalist MACE-MP-0 trained with ~10^6 structures [30], with errors being more than an order of magnitude smaller. Similarly, we trained MACE models with a BTO and combined CTO+BTO+CZO datasets. Figure 2b compares the energy prediction for the soft phonon mode of $BaTiO_3$, again showing that specialized models give better predictions than MACE-MP-0. Note that MACE-MP-0 captures the energy profile near equilibrium quite well, but underestimates the energy away from equilibrium. The larger discrepancies for MACE-MP-0 may be partly due to the different functional being used (PBEsol here vs. PBE in MPtrj), as well

as difference in values for the Hubbard *U* correction. Still, the model performs surprisingly well for not being specifically trained with these configurations. Also note that the soft mode of BTO, for which long range electrostatic interactions play a great role, is captured well by MACE, despite being a local force field.

In order to obtain the polarization in the external field, a combined force field equal to the sum of MACE and Equivar was used, according to eqs 1-2. Total polarization is obtained from the Born charges and atomic displacements due to forces from the external field. Figure 3 shows the calculated static polarization of CTO for fields $0<E<10^8$ V/m. The softer MACE-MP-0 force field predicts larger polarization, and faster onset of nonlinearity compared to model 'A'. The predictions of the *P* values are seen to be more sensitive to the choice of the MACE force field than the Born charge model. The efficient and accurate GCNN force fields enable fast simulations of large systems. In particular, statistical sampling for each atom, normally computationally prohibitive and restricted to model systems, becomes possible for realistic crystals. We test the capability of the force field to predict structural phase transitions in CTO. Experimentally, CTO undergoes two phase transitions, from orthorhombic to tetragonal, and from tetragonal to cubic structures, as temperature increases. The respective transition temperatures are 1512 ± 13 K and 1635 ± 2 K [39]. We performed *NpT* simulations using the 640-atom 4×4×2 and 1280-atom 4×4×4 supercells, and a heating rate of 1 K/ps, between 300 K and 1800 K.

The results of the heating simulations are compared with the experimental data in Fig. 4. Unlike experimental observations, a single phase transition from the orthorhombic to cubic phase occurs in the simulation, and no tetragonal phase is observed. During heating, the system switched from the orthorhombic to cubic phase and back, before adopting the symmetric cubic structure. The approximate temperature of the phase transition in the simulated system is around 1280 K. The system shows linear expansion throughout the range of temperatures tested, similar to experiment. Note that the structural phase transitions in CTO are rather subtle, and different transition temperatures as well as the presence of another orthorhombic phase have been reported in previous experiments, as summarized in Table I of Ref. [40]. The lower predicted phase transition temperature and the absence of the tetragonal phase could also be due to error inherent in the approximate density functional used for the training set creation, and not indicative of the model accuracy.

Finally, we demonstrate finite temperature molecular dynamics simulations to evaluate the dielectric tensor of CTO. Experimentally, it is known to decrease with increasing temperature, depicted by a characteristic bell-shaped curve [41]. We performed MD simulations of CTO at finite *T* and recorded a full dielectric tensor by time averaging the polarization at each temperature for each direction of the electric field parallel to the axes of the Cartesian coordinate system. The resulting diagonal components are shown in Fig. 5. In Fig. 5a, averaging at each temperature was performed over 1000 frames collected from a 10 ps run in a primitive 20-atom unit cell; in Fig. 5b, the averaging was performed for 5000 frames from a 50 ps run in a 2×2×1 80-atom supercell. The latter results contain much less noise, which allows observing the anisotropy of the dielectric tensor clearly. Note that in the higher temperature region where the dielectric tensor components are smaller, imposing from the translational symmetry with a small unit cell induces significant errors. The simulations are also seen to reproduce the decreasing trend and also the shape of the experimental curve. Zero temperature

results are smaller than the DFPT values, most likely due to nonlinearity of polarization with the external electric field. It is seen from Fig. 3 that polarization curves bend down as electric field increases, leading to smaller response than that given by DFPT with infinitesimal field. Also note that the theoretical values are smaller than experimental ones due to the limitations of density functionals used to generate the ground truth set. Also, the low temperature plateau stemming from the quantum mechanical zero point motion, is absent. This effect cannot be captured in classical simulations and requires a quantum mechanical description of the nuclear motion.

4. Conclusions

We demonstrate the application of force fields based on equivariant graph neural networks to finite temperature MD simulations of realistic materials in external electric fields. MACE and Equivar models trained on small datasets of perovskite oxides show better performance than the generalist models trained on much larger sets. Using these models, total energies, forces and tensors of dynamic Born effective charges are obtained with close to ab initio accuracy, and molecular dynamics simulations at finite temperatures and in finite electric fields are performed. The decrease of the dielectric tensor with temperature and structural phase transition from orthorhombic to cubic phase are captured qualitatively in calcium titanate.

The proposed method will open the door to vast applications such as inhomogeneous dielectric systems like relaxor and multilayer/heterostructure systems, which are not accessible by either classical or ab-initio simulations. Recently, equivariant GCNNs, where the Born effective charges were evaluated by the derivatives of the polarization with respect to the atomic displacement, were applied to study ferroelectric properties of $BaTiO_3$ [15]. In contrast, the present Equivar model directly predicts the Born effective charges, and the hybrid model with the force field GNN model has an opportunity of flexible design and training for each model to improve accuracy and applicability. The latter feature may be particularly useful when pretrained force-field models become more available in future.

Data availability statement

The python scripts for running the Equivar model for prediction of Born effective charges tensor can also be downloaded from https://github.com/equivar/equivar_eval/

Disclosure statement

No potential conflict of interest was reported by the author(s).

Funding

The work was supported by the JSPS Grant-in-Aid for Transformative Research Areas (A) (23H04105).

References

[1] Reiser P, Neubert M, Eberhard A, et al. Graph neural networks for materials science and chemistry. Commun. Mater. 2022;3:93. doi: 10.1038/s43246-022-00315-6

[2] Gilmer J, Schoenholz S S, Riley P F, et al. Neural Message Passing for Quantum Chemistry. In: *Proceedings of the 34th International Conference on Machine Learning* Proceedings of Machine Learning Research; 2017. vol 70, ed D Precup and Y W Teh (PMLR) pp 1263–72

[3] Cohen T and Welling M Group Equivariant Convolutional Networks. In: *Proceedings of The 33rd International Conference on Machine Learning* Proceedings of Machine Learning Research; 2016. vol 48, ed M F Balcan and K Q Weinberger (New York, New York, USA: PMLR) pp 2990–9

[4] Thomas N, Smidt T, Kearnes S, et al. Tensor field networks: Rotation- and translation-equivariant neural networks for 3D point clouds. 2018. Available from: https://arxiv.org/abs/1802.08219

[5] Batzner S, Musaelian A, Sun L, et al. E(3)-equivariant graph neural networks for data-efficient and accurate interatomic potentials. Nat. Commun. 2022;13:2453. doi: 10.1038/s41467-022-29939-5

[6] Batatia I, Kovacs D P, Simm G, et al. MACE: Higher Order Equivariant Message Passing Neural Networks for Fast and Accurate Force Fields. In: *Advances in Neural Information Processing Systems*; 2022. vol 35, ed S Koyejo, S Mohamed, A Agarwal, D Belgrave, K Cho and A Oh (Curran Associates, Inc.) pp 11423–36

[7] Schütt K, Unke O and Gastegger M Equivariant message passing for the prediction of tensorial properties and molecular spectra. In: *Proceedings of the 38th International Conference on Machine Learning* Proceedings of Machine Learning Research; 2021. vol 139, ed M Meila and T Zhang (PMLR) pp 9377–88

[8] Okabe R, Chotrattanapituk A, Boonkird A, et al. Virtual node graph neural network for full phonon prediction. Nat. Comput. Sci. 2024;4:522–31. doi: 10.1038/s43588-024-00661-0

[9] Cheng Y, Wu G, Pajerowski D M, et al. Direct prediction of inelastic neutron scattering spectra from the crystal structure. Mach. Learn. Sci. Technol. 2023;4:015010. doi: 10.1088/2632-2153/acb315

[10] Vijay S, Venetos M C, Spotte-Smith E W C, et al. CoeffNet: predicting activation barriers through a chemically-interpretable, equivariant and physically constrained graph neural network. Chem Sci. 2024;15:2923–36. doi: 10.1039/D3SC04411D

[11] Kutana A, Shimizu K, Watanabe S, et al. Representing Born effective charges with equivariant graph convolutional neural networks. 2024; doi: 10.48550/arXiv.2409.08940 Available from: https://arxiv.org/abs/2409.08940

[12] Koji Shimizu E M Ryuji Otsuka, Masahiro Hara and Watanabe S Prediction of Born effective charges using neural network to study ion migration under electric fields: applications to crystalline and amorphous Li3PO4. Sci. Technol. Adv. Mater. Methods. 2023;3:2253135. doi: 10.1080/27660400.2023.2253135

[13] Malenfant-Thuot O, Ryczko K, Tamblyn I, et al. Efficient determination of Born-effective charges, LO-TO splitting, and Raman tensors of solids with a real-space atom-centered deep learning approach. J. Phys. Condens. Matter. 2024;36:425901. doi: 10.1088/1361-648X/ad64a2

[14] Schmiedmayer B and Kresse G Derivative learning of tensorial quantities—Predicting finite temperature infrared spectra from first principles. J. Chem. Phys. 2024;161:084703. doi: 10.1063/5.0217243

[15] Falletta S, Cepellotti A, Johansson A, et al. Unified Differentiable Learning of Electric Response. 2024. Available from: https://arxiv.org/abs/2403.17207

[16] Umeda Y, Hayashi H, Moriwake H, et al. Prediction of dielectric constants using a combination of first principles calculations and machine learning. Jpn. J. Appl. Phys. 2019;58:SLLC01. doi: 10.7567/1347-4065/ab34d6

[17] Takahashi A, Kumagai Y, Miyamoto J, et al. Machine learning models for predicting the dielectric constants of oxides based on high-throughput first-principles calculations. Phys Rev Mater. 2020;4:103801. doi: 10.1103/PhysRevMaterials.4.103801

[18] Shimano Y, Kutana A and Asahi R Machine learning and atomistic origin of high dielectric permittivity in oxides. Sci. Rep. 2023;13:22236. doi: 10.1038/s41598-023-49603-2

[19] Kim E, Kim J and Min K Prediction of dielectric constants of ABO3-type perovskites using machine learning and first-principles calculations. Phys Chem Chem Phys. 2022;24:7050–9. doi: 10.1039/D1CP04702G

[20] Morita K, Davies D W, Butler K T, et al. Modeling the dielectric constants of crystals using machine learning. J. Chem. Phys. 2020;153:024503. doi: 10.1063/5.0013136

[21] Chen L, Kim C, Batra R, et al. Frequency-dependent dielectric constant prediction of polymers using machine learning. Npj Comput. Mater. 2020;6:61. doi: 10.1038/s41524-020-0333-6

[22] M. Gori, G. Monfardini, and F. Scarselli A new model for learning in graph domains. *Proceedings. 2005 IEEE International Joint Conference on Neural Networks, 2005.* Proceedings. 2005 IEEE International Joint Conference on Neural Networks, 2005. vol 2 pp 729–34 vol. 2

[23] Schütt K T, Sauceda H E, Kindermans P-J, et al. SchNet – A deep learning architecture for molecules and materials. J. Chem. Phys. 2018;148:241722. doi: 10.1063/1.5019779

[24] Geiger M and Smidt T e3nn: Euclidean Neural Networks. 2022. Available from: https://arxiv.org/abs/2207.09453

[25] Kondor R, Lin Z and Trivedi S Clebsch– Gordan Nets: a Fully Fourier Space Spherical Convolutional Neural Network. In: *Advances in Neural Information Processing Systems*; 2018. vol 31, ed S Bengio, H Wallach, H Larochelle, K Grauman, N Cesa-Bianchi and R Garnett (Curran Associates, Inc.)

[26] Kresse G and Furthmüller J Efficiency of ab-initio total energy calculations for metals and

semiconductors using a plane-wave basis set. Comput. Mater. Sci. 1996;6:15–50. doi: http://dx.doi.org/10.1016/0927-0256(96)00008-0

[27] Kutana A, Shimano Y and Asahi R Permittivity boosting by induced strain from local doping in titanates from first principles. Sci. Rep. 2023;13:3761. doi: 10.1038/s41598-023-30965-6

[28] Nunes R W and Gonze X Berry-phase treatment of the homogeneous electric field perturbation in insulators. Phys Rev B. 2001;63:155107. doi: 10.1103/PhysRevB.63.155107

[29] Batatia I, Benner P, Chiang Y, et al. A foundation model for atomistic materials chemistry. 2023. Available from: https://arxiv.org/abs/2401.00096

[30] Deng B, Zhong P, Jun K, et al. CHGNet as a pretrained universal neural network potential for charge-informed atomistic modelling. Nat. Mach. Intell. 2023;5:1031–41. doi: 10.1038/s42256-023-00716-3

[31] Posternak M, Resta R and Baldereschi A Role of covalent bonding in the polarization of perovskite oxides: The case of $KNbO_3$. Phys Rev B. 1994;50:8911–4. doi: 10.1103/PhysRevB.50.8911

[32] Ph. Ghosez X G and Michenaud J-P A microscopic study of barium titanate. Ferroelectrics. 1995;164:113–21. doi: 10.1080/00150199508221833

[33] Ghosez P, Michenaud J-P and Gonze X Dynamical atomic charges: The case of ABO_3 compounds. Phys Rev B. 1998;58:6224–40. doi: 10.1103/PhysRevB.58.6224

[34] Cohen R E and Krakauer H Lattice dynamics and origin of ferroelectricity in BaTiO3: Linearized-augmented-plane-wave total-energy calculations. Phys Rev B. 1990;42:6416–23. doi: 10.1103/PhysRevB.42.6416

[35] Cohen R E Origin of ferroelectricity in perovskite oxides. Nature. 1992;358:136–8. doi: 10.1038/358136a0

[36] Resta R and Vanderbilt D Theory of Polarization: A Modern Approach. *Physics of Ferroelectrics: A Modern Perspective* (Berlin, Heidelberg: Springer Berlin Heidelberg); 2007. pp 31–68

[37] Zhong W, King-Smith R D and Vanderbilt D Giant LO-TO splittings in perovskite ferroelectrics. Phys Rev Lett. 1994;72:3618–21. doi: 10.1103/PhysRevLett.72.3618

[38] Cockayne E and Burton B P Phonons and static dielectric constant in CaTiO3 from first principles. Phys Rev B. 2000;62:3735–43. doi: 10.1103/PhysRevB.62.3735

[39] Yashima M and Ali R Structural phase transition and octahedral tilting in the calcium titanate perovskite CaTiO3. Solid State Ion. 2009;180:120–6. doi: 10.1016/j.ssi.2008.11.019

[40] Ali R and Yashima M Space group and crystal structure of the Perovskite CaTiO3 from 296 to 1720K. J. Solid State Chem. 2005;178:2867–72. doi: 10.1016/j.jssc.2005.06.027

[41] Lemanov V V, Sotnikov A V, Smirnova E P, et al. Perovskite CaTiO3 as an incipient ferroelectric. Solid State Commun. 1999;110:611–4. doi: 10.1016/S0038-1098(99)00153-2

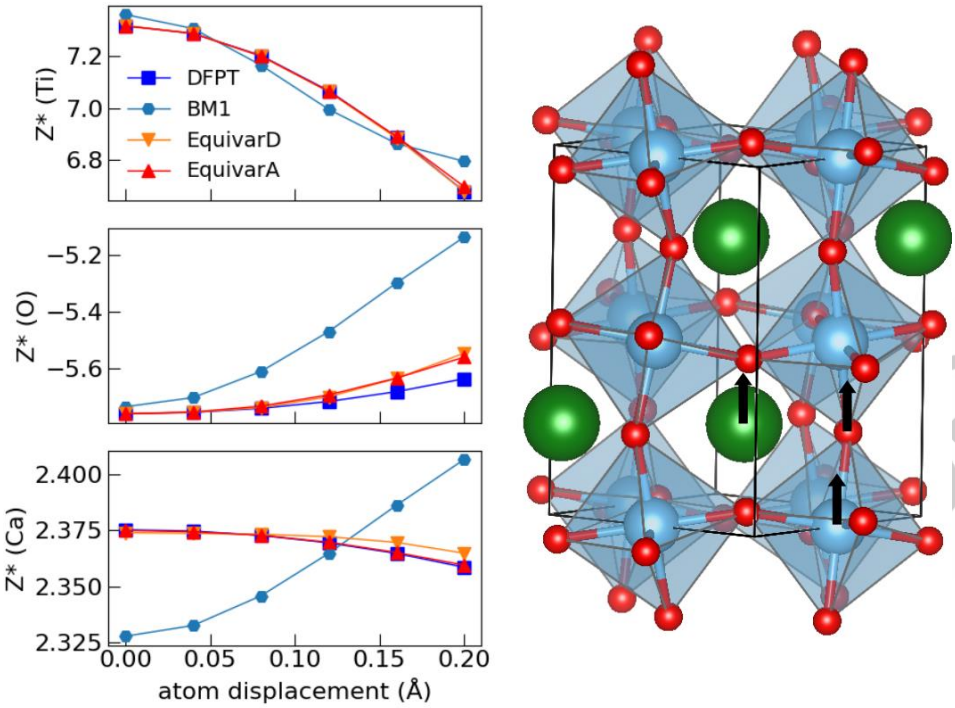

Figure 1. Dynamic charges for single atom displacements in $CaTiO_3$ computed with DFPT and different Equivar models. Displacements are in the direction of the *z* axis, as shown by the arrows in the panel on the right.

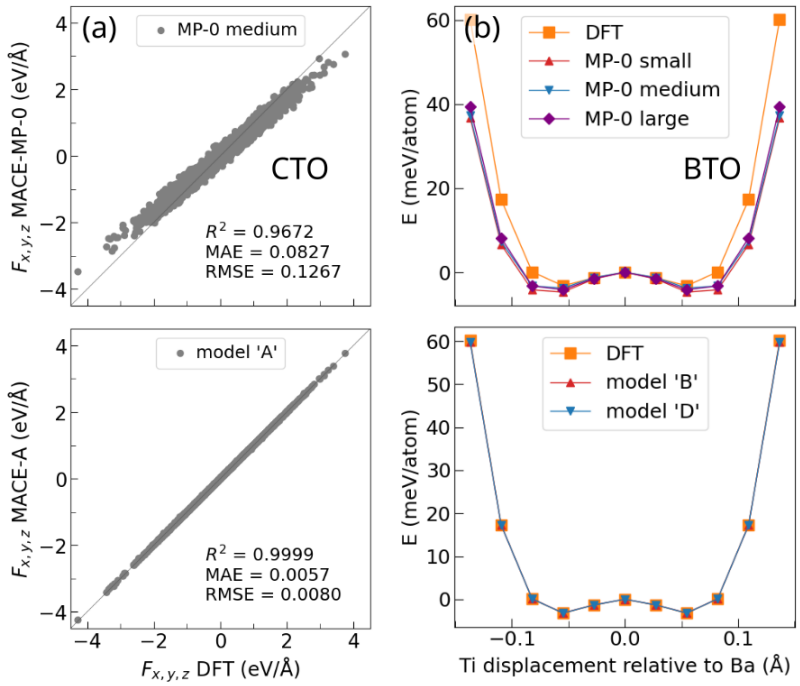

Figure 2. (a) Force parity plots for MACE-MP-0 (upper panel), and five-fold cross-validation of MACE model 'A' trained on the CTO dataset (lower panel) with PBESol DFT forces as a ground truth; (b) energy profiles for the displacement along the soft phonon mode in cubic $BaTiO_3$ using MACE-MP-0 (upper panel) and MACE models 'B' and 'D' (lower panel). PBESol DFT energies are also shown.

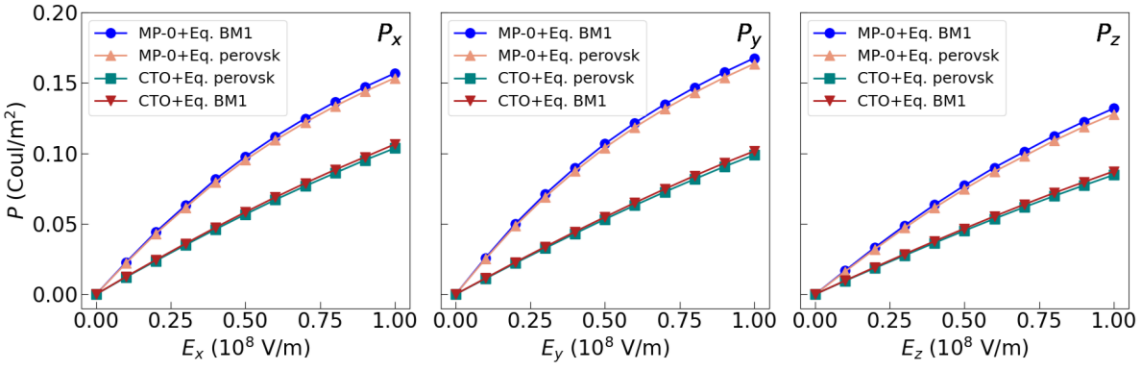

Figure 3. Polarization of $CaTiO_3$ in the applied electric field. The results for the MP-0 and custom trained MACE models are shown. From the slopes, the static dielectric tensor is obtained. MP-0 force field underestimates the force constants and overestimates the nonlinearity.

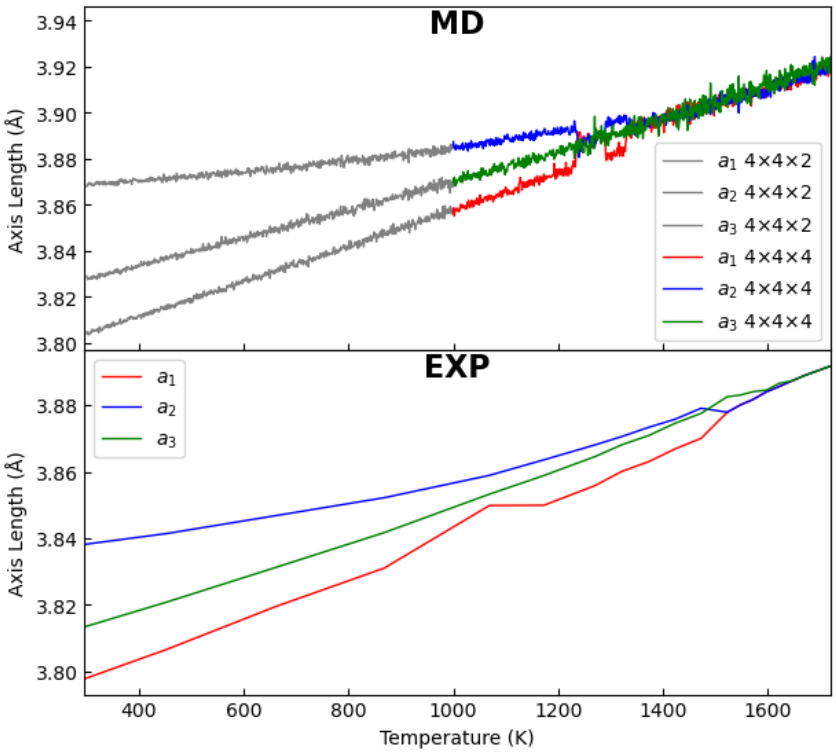

Figure 4. Structural phase transitions in $CaTiO_3$ from heating simulations and experimental data. Top panel shows the computed curves, and bottom panel experimental data [39]. In the upper panel, the gray lines show results for the 4×4×2 simulation cell, and color lines for the 4×4×4 cell.

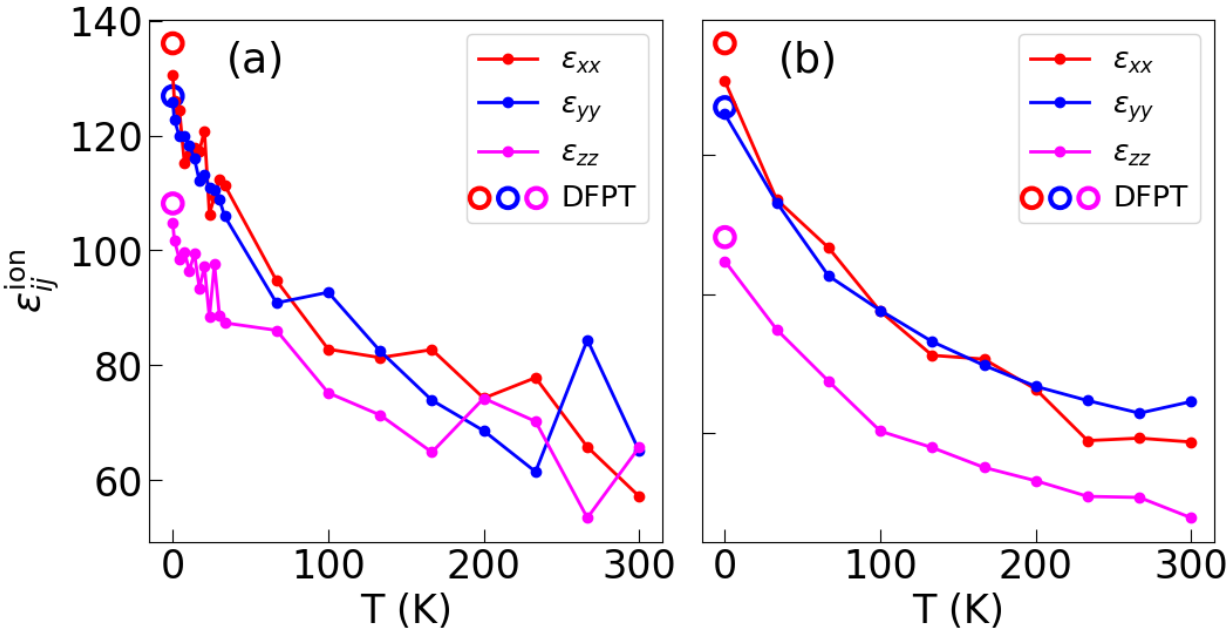

Figure 5. Temperature-dependent ionic dielectric tensor of $CaTiO_3$. The values from the finite temperature MD simulations are shown with filled circles. (a) averaging was performed over 1000 frames from a 10 ps run in a primitive 20-atom unit cell at each temperature; (b) averaging was performed over 5000 frames from a 50 ps run in a 2×2×1 supercell at each temperature. Zero temperature DFPT values are shown with empty circles.

Impact_Statement

The newly developed hybrid GNN model to predict a force field and Born effective charges successfully enables to simulate temperature-dependent anisotropic dielectric tensor from finite temperature MD simulations.

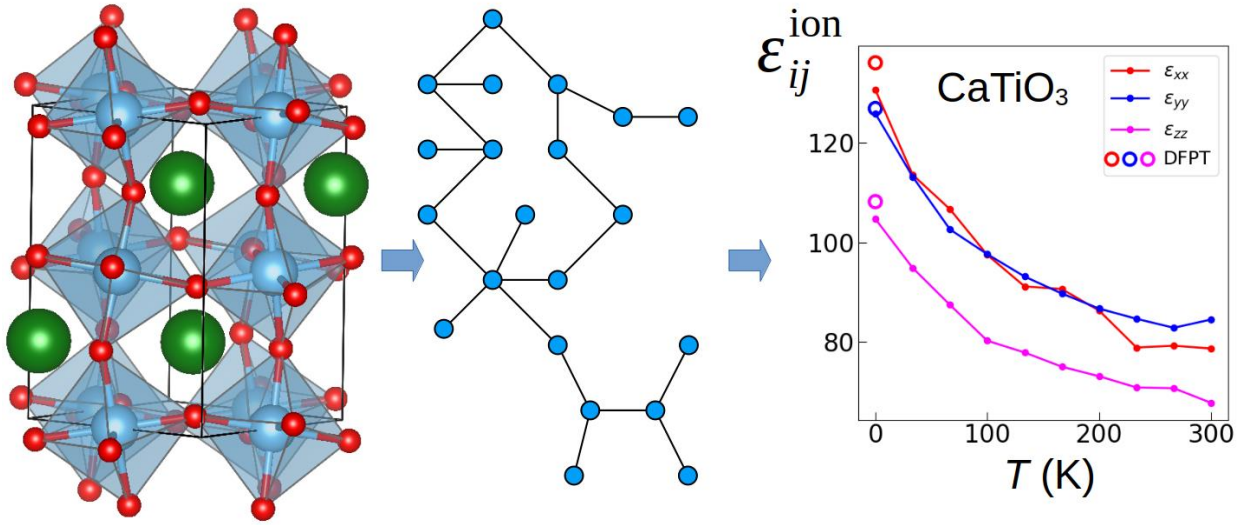

Graphical abstract

Supplemental Material for: “Dielectric tensor of perovskite oxides at finite temperature using equivariant graph neural network potentials”

Alex Kutana, Koki Yoshimochi and Ryoji Asahi ✉

Nagoya University, Furo-cho, Chikusa-ku, Nagoya, Japan
✉E-mail: asahi.ryoji.d9@f.mail.nagoya-u.ac.jp

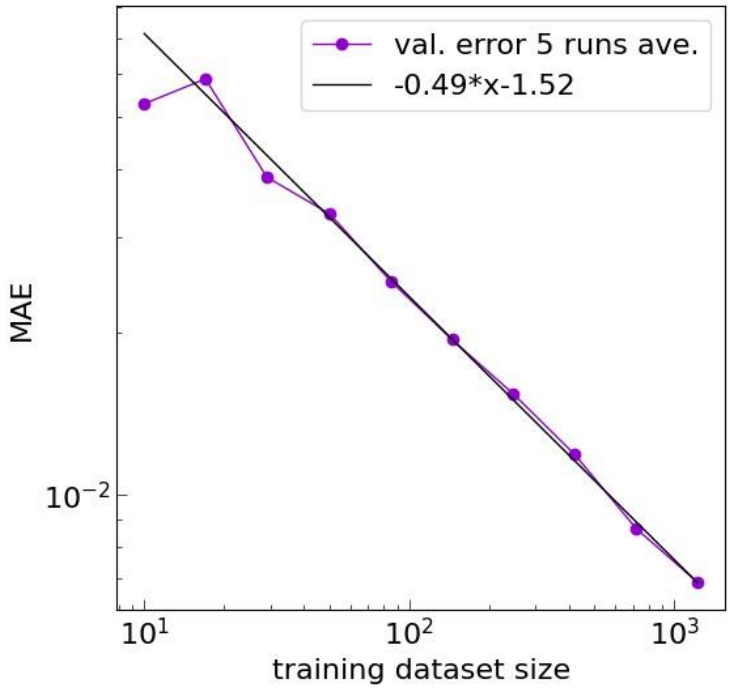

Figure S1. Learning curve of Equivar for the perovskites dataset.